ARTICLES

Epitaxial-strain-stabilized ordering in $Au_{1-x}Ni_x$ alloy thin films grown by MBE

G. Abadias,* I. Schuster, and A. Marty

CEA-Grenoble, Département de Recherche Fondamentale sur la Matière Condensée, SP2M, 17 Avenue des Martyrs, 38054 Grenoble cedex 09, France

B. Gilles

LTPCM-ENSEEG, Institut National Polytechnique de Grenoble, 38402 Saint Martin d'Hères cedex, France

The influence of the epitaxial strain on the structural evolution with temperature of AuNi metastable alloys thin films is investigated. Samples with different initial configurations (codeposited $Au_{1-x}Ni_x$ solid solutions and artificially layered structures) were grown by molecular-beam epitaxy on different (001)-oriented buffer layers (Au, Pt, and Pd). The epitaxial strain was varied by changing (i) the Ni content of the AuNi layer for a given kind of buffer layer, (ii) the nature of the buffer layer for a fixed Ni content, and (iii) the AuNi layer thickness for a fixed Ni content and buffer layer. The structural evolution upon annealing in the 180–300 °C temperature range was studied by *in situ* temperature x-ray diffraction as well as high-resolution electron microscopy. It is shown that a modulated structure develops along the growth direction of the AuNi layer, when the temperature reaches 200–240 °C, provided that the residual strain is high enough (>2%). This structure consists of a periodic stacking of 1 Ni-rich plane and 2 or 3 Au-rich planes, depending on the Ni content. The results are explained in terms of a strain-stabilized ordering effect, as supported by energetic calculations based on semiempirical interatomic potentials within the tight-binding scheme.

I. INTRODUCTION

Obtaining materials in a nonequilibrium state or with artificial structures has always been an attractive challenge in materials science research for the novel physical properties that may be hoped for. Nonthermodynamic (metastable) phases may be formed by using classical metallurgical ways (quenching and annealing) or during irradiation processes. But employing epitaxial growth to induce such metastable materials has been gathering much attention in the last decade[1–12] since accurate control of the film growth is possible on an atomic scale.[13] Peculiar phenomena to molecular beam epitaxy (MBE) have been reported in the literature: these include (i) structural phase transitions,[1,2] (ii) the stabilization of new ordered compounds,[3–6] or (iii) alloying in systems where the materials are immiscible in their bulk forms.[7–9] These phenomena are essentially governed by a *strain effect* due to the lattice mismatch between the substrate (or the buffer layer) and the deposited thin film, as supported by theoretical calculations.[10,11,14] But specific effects occurring during the epitaxial growth process also have to be taken into account: they involve surface diffusion and segregation mechanisms.[9,12,15]

In the case of the AuNi system to which the present work is dedicated, the two elements have the same fcc structure but their lattice cell parameters differ by 14% ($a_{Au}=4.08$ Å, $a_{Ni}=3.52$ Å), thus indicating that a high strain effect may be expected. The solid-state portion of the bulk equilibrium phase diagram (see Fig. 1) exhibits a wide asymmetrical miscibility gap with almost no solubility at room

temperature (RT).[16] The out-of-equilibrium AuNi system was first studied through quenched bulk alloys:[17] metastable disordered fcc AuNi solid solutions have been obtained for the whole composition range at RT by rapid quenching from a temperature at which the single-phase AuNi mixture is the equilibrium state. $Au_{1-x}Ni_x$ solid solutions thin films have also been obtained at RT by a MBE growth on a Au(001) buffer layer,[7] with atomic fractions of Ni up to $x=0.6$, i.e., much above the bulk solubility ($\sim$0.01). The strain effect is probably the dominant effect in this alloying mechanism since large epitaxial stresses are expected to lower drastically the miscibility gap[18–19] (see the dashed curve of Fig. 1) and
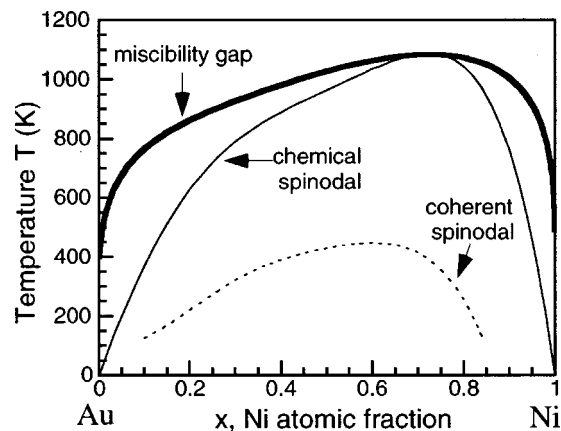
FIG. 1. Bulk equilibrium AuNi phase diagram calculated from Ref. 19: miscibility gap (——), chemical spinodal (——) and coherent spinodal (— — —).

also because kinetic effects are limited at RT due to the low atomic mobility of the incoming atoms.

The study of the structural evolution of these metastable AuNi alloys upon annealing takes on particular importance in order to determine the evolving path towards the equilibrium state.

In the bulk state, periodic compositional modulations[20–22] have been observed during annealing below 300 °C. The reported modulations were along the three $\langle 100 \rangle$ directions, with a period depending on the Ni content and with an amplitude estimated to be a few percent.[20] It has been suggested that these modulated structures may result from a spinodal decomposition mechanism although, in some cases, they do not evolve towards phase separation during the later stages, as predicted by Cahn's formal theory of the spinodal decomposition.[23] Renaud *et al.*[24] have suggested that the process may be blocked for thermodynamical reasons linked to the anharmonicity of the elastic contribution to the mixing energy: the compositional modulations induce large structural distortions, which rapidly increase the elastic energy. The chemical energy gain is therefore reduced and the evolution is stopped.

We have shown in a recent paper[25] that periodic compositional modulations also develop upon annealing of AuNi epitaxial ultrathin films grown on Au (001), but only along the growth direction due to the biaxial stress. The variation of the period with the Ni content is consistent with the one observed in the bulk state in the same temperature range. However the composition amplitude is greater (over 40%) and no evolution of the period with temperature and time is observed, which may indicate that an ordering process takes place rather than a spinodal decomposition mechanism.

In both cases, the elastic strain seems to play a leading part in the appearance and evolution of the modulated structures. The aim of this paper is to detail the influence of the epitaxial strain on the structural evolution in temperature of AuNi thin films and to understand the involved mechanisms. For this purpose, experiments were undertaken on several MBE-grown AuNi alloys with different compositions, states of strain and initial configurations. The structural characterization was performed using *in situ* temperature x-ray diffraction (XRD) as well as high resolution electron microscopy (HREM). The paper is organized as follows: section II is devoted to thermodynamical considerations on the stability of the AuNi system in the bulk state and under epitaxial constraints. Section III describes the samples preparation and Sec. IV the structural evolution upon annealing. The whole results are discussed in Sec. V by comparing them to numerical simulations.

II. THERMODYNAMICAL CONSIDERATIONS

A. Bulk state

The thermodynamics of the AuNi system has been widely studied[26–34] because of its peculiar energetic and elastic features, which makes it a testing ground for theories of alloy stability. Indeed, the large size mismatch makes the effect of atomic relaxation critical and despite a strong phase-separation tendency at low temperature and positive mixing enthalpies,[35] an ordering-type short-range order (SRO) has been observed experimentally.[26,36] This surprising behavior
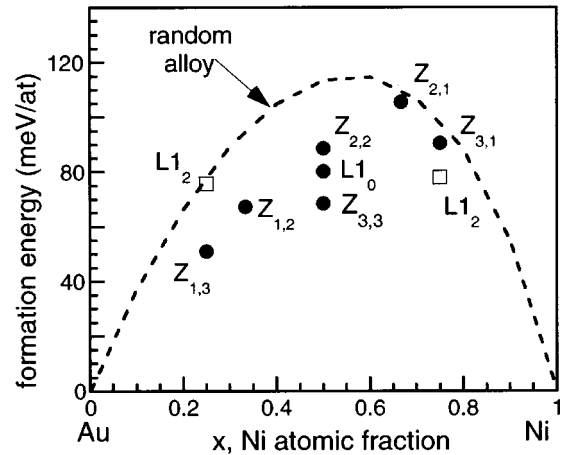
FIG. 2. Calculated formation energy (at $T = 0$ K) of disordered fcc $Au_{1-x}Ni_x$ solid solutions (dashed line) and of $Z_{n,m}$ type ordered structures (symbols).

has been clarified by Wu and Cohen:[27] they have determined, from experimental data, the chemical and elastic contribution to the mixing energy of a $Au_{0.6}Ni_{0.4}$ alloy at $T = 1083$ K, i.e., just above the miscibility gap. They found that (1) the chemical energy is slightly negative ($\Delta E_{ch} = -0.63$ kJ/mol) indicating an ordering tendency and (2) the elastic energy is large and positive ($\Delta E_{elas} = 8.45$ kJ/mol) making the total mixing energy $\Delta E_{mix} = \Delta E_{ch} + \Delta E_{elas}$ positive.

These results have been confirmed theoretically by computational models based on first-principles calculations—full potential linear muffin-tin orbitals (FP-LMTO),[31] full potential linearized augmented plane-wave (FLAPW)[32,33]—or semiempirical potentials within the tight binding (TB) scheme[31] (for details on the interatomic potential, see Refs. 28 and 37). In both methods, the ground state is found to be the phase-separated alloy and a tendency to SRO ordering exists, given by the negative sign of the ordering energy $\Delta E_{ord}(\sigma_x)$ of Ni_nAu_m (001) ordered structures, where $\Delta E_{ord}(\sigma_x)$ is defined as the difference between the formation energy $\Delta E(\sigma_x)$ of the ordered compound in the σ structure and the mixing energy ΔE_{mix} of the random alloy of the same composition. But the calculations based on the semiempirical potentials, though convenient for treating systems with a large number of atoms and configurations, give values of $\Delta E(\sigma_x)$ and ΔE_{mix} smaller than those predicted from first-principles (accurate but time-consuming) methods, indicating that the chemical effects are not properly taken into account. To overcome this deficiency, the heteroatomic terms of the TB potential developed by Deutsch *et al.*[37] were adjusted to reproduce the energy values of Ref. 31 calculated from FP-LMTO. The adjustments[38] were performed on a set of metastable ordered structures: $Au_3Ni(L1_2)$, $AuNi_3(L1_2)$, $AuNi(L1_0)$ and AuNi (Z2). The transferability of the potential adjusted in this way was tested on several other structures, mainly Ni_n/Au_m superlattices along the $\langle 001 \rangle$ direction, which is the elastically soft direction for Au/Ni coherent layers.[39] Good agreement was obtained with the first-principles results.

The values at $T = 0$ K of the mixing energy ΔE_{mix} of random alloys are reported on Fig. 2 as well as the formation energy of some ordered compounds: $L1_2(Au_3Ni)$, $L1_2(AuNi_3)$, $L1_0$, ``$Z_{2,2}$'', ``$Z_{3,3}$'', ``$Z_{1,2}$'', ``$Z_{1,3}$'',

''$Z_{2,1}$'', and ''$Z_{3,1}$'', where the notation ''$Z_{n,m}$'' refers to Ni_n/Au_m superlattices along the $\langle 001 \rangle$ direction. Several relevant points may be stressed:

(i) The value of ΔE_{mix} ($x=0.5$) is 113 meV/at, very close to the value obtained from FLAPW (Ref. 32) (118 meV/at), but higher than the experimental value[35] (76 meV/at) measured at 1150 K, i.e., just above the miscibility gap where a SRO has been reported. Wolverton and Zunger[32] have shown, by Monte Carlo simulations, that taking into account SRO lowers the mixing energy by ~25 meV/at. We can therefore estimate to 88 meV/at the value of $\Delta E_{mix}(x=0.5)$, i.e., close to the experimental value. (ii) $Z_{n,m}$ (including $L1_0$) and $L1_2$ ordered structures are metastable phases: their energy is lower than that of the random alloy but higher than the phase-separated state. Consequently, both $\langle 001 \rangle$ ordering-type and clustering-type fluctuations of the random alloy may be expected. (iii) The ordering energy of $Z_{1,n}$ ($n > 1$) structures is much lower than that of $Z_{n,1}$ ones. Thus, if an ordering may occur, ordered structures with the alternation of 1 Ni plane / 2 or 3 Au planes are more favorable than those with an alternation of 1 Au plane / 2 or 3 Ni planes.

B. Epitaxial effects

Under epitaxial constraints, the phase equilibria in the AuNi system are expected to be drastically altered by the elastic strain energy required to accommodate the substrate and the deposited film lattices, due to the large size effect.

Ozolins et al.[39] have calculated from first-principles the stability of *elemental* epitaxial films (pure Au and Ni films coherently grown on a substrate). Their description of the elastic strain energy takes into account anharmonic effects. It is noteworthy that, for pure Ni film, they found that under biaxial tension, the $\langle 001 \rangle$ axis is the soft direction and under compression the soft direction changes to $\langle 201 \rangle$. This ''epitaxial softening'' along $\langle 001 \rangle$ is a consequence of geometric properties of the $\langle 001 \rangle$ ''epitaxial Bain path'' (connecting cubic symmetry fcc and bcc structures),[40,41] and a low bcc/fcc energy differences. For Ni, a local minimum is found for a bct structure with an in-plane lattice parameter very close to that of Au.[42] As a direct consequence, when growing Ni_n/Au_m superlattices, the system rich in Au ($m > n$) will have a low $\langle 001 \rangle$ elastic energy due to the easy expansion of Ni on Au. Experimentally, (Ni_n/Au_{20}) multilayers have been grown coherently by MBE on Au (001) for $n < 4$.[42,43] This stabilization may be explained in terms of an epitaxial softening in agreement with the calculations of Ozolins et al. But an alloying effect driven by surface segregation mechanisms also occurs during growth.[37,43]

Regarding the stability of epitaxial *alloys*, the only available data in the literature correspond to random alloys.[19] The calculations were performed within Cahn's continuum model and cannot predict the stability of ordered compounds. To account for both random alloys and ordered compounds on the same footing, we have used a cluster-based description of coherent binary alloys, according to the basic model of Wood and Zunger.[11] We have worked within the tetrahedron approximation and used the TB interatomic potentials described above to calculate the energetic and elastic inputs. Details of the calculations will be presented in a separate publication.[38] We have calculated the formation energies of
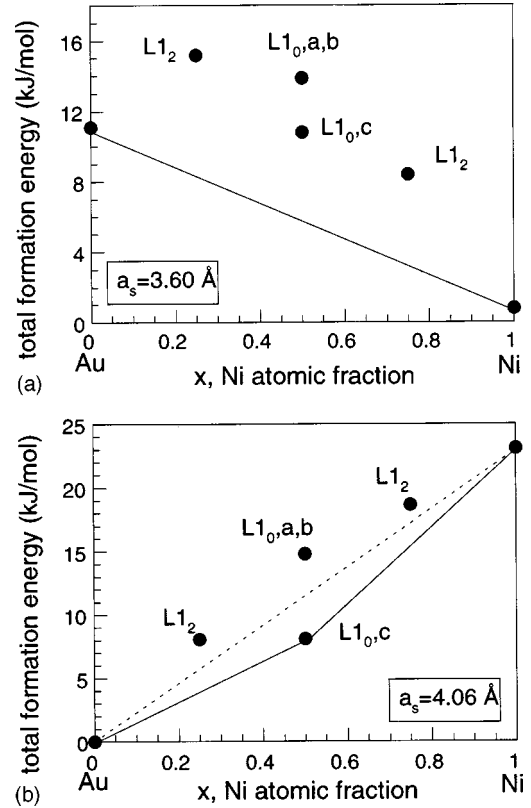
FIG. 3. Calculated total formation energy (at $T=0$ K) of some ordered compounds under epitaxial constraints: (a) $a_s = 3.60$ Å and (b) $a_s = 4.06$ Å.

some simple structures epitaxially strained on a (001)-oriented substrate having a lattice parameter a_s: A1 (pure Au and Ni), $L1_2$ (Ni_3Au and Au_3Ni) with cubic symmetry and $L1_0$ with tetragonal symmetry. The three variants of the $L1_0$ structure are noted a, b, and c for the respective orientations $\langle 100 \rangle$, $\langle 010 \rangle$, and $\langle 001 \rangle$.

The results are reported on Fig. 3, which displays the ground state at $T=0$ K of the epitaxial AuNi system for two substrate lattice parameters: $a_s = 3.60$ Å (Ni-rich) and 4.06 Å (Au-rich). For $a_s = 3.60$ Å, phase separation is expected to occur since the ground state is Au+Ni. For $a_s = 4.06$ Å, the $L1_0$ structure with the variant along the $\langle 001 \rangle$ direction becomes a stable state at $T=0$ K for $x=0.5$. Thus an $L1_0$-type ordering may be obtained in epitaxial $Au_{0.5}Ni_{0.5}$ alloys grown on Au (001). Our calculations[38] show that there exist a threshold strain for the $L1_0$ structure to become stable, which corresponds to a value of $a_s = 3.95$ Å. In addition, ordered structures with cubic symmetry (such as $L1_2$) are energetically unfavorable under a biaxial constraint due to their high elastic epitaxial strain energy.

III. EXPERIMENTAL DATA

A. Growth

The samples were grown by MBE in an ultrahigh vacuum chamber in which the base pressure was approx. 10^{-10} Torr. The deposition at RT of the materials was carried out using two electron beam evaporators of pure Au and Ni sources and controlled using quartz microbalances. Sample growth was monitored using reflection high energy electron diffrac-

tion (RHEED) operating at 40 kV and an angle of incidence of 1.5°. The AuNi alloy layers were grown on a 50 nm-thick (001) buffer layer,[44] this latter being deposited on a MgO (001)-oriented substrate via a 3 nm-thick Fe seed layer.[45] The pressure in the MBE chamber rose to approx. 10^{-9} Torr during the deposition of the AuNi or the buffer layers.

The MgO (001) substrates used for sample growth were simply degreased before the transfer into the MBE system, where they were heated at 150 °C for 1 h to remove water from the surface, then at 350 °C for 3 h to remove miscellaneous hydrocarbons and finally at 450 °C for 0.5 h to make chlorine radicals desorb. Growth began with the deposition at RT of the Fe seed layer at a rate of 0.5 Å/s, immediately followed by the deposition of the buffer layer (Au, Pt, or Pd) at a rate of 1 Å/s, again at RT. Prior to the deposition of the AuNi layers, the buffer layer was heated for 10 mn at 400 °C in order to have a smooth surface, which has the classical (1×5) reconstruction[46] for the case of Au or Pt. The AuNi alloy was then grown by coevaporating the Au and Ni sources at a growth rate ranging from 0.3 Å/s to 0.6 Å/s depending on the chosen composition. The AuNi film was finally covered by a capping layer of the same nature than that of the buffer layer. This ensures the same state of strain both at the top and at the bottom interface of the AuNi layer. For the three different types of buffer layers used in this study, the RHEED pattern reveals the cube-on-cube epitaxial relationship [001] (001) buffer // [001] (001) AuNi. In addition, no significant C or O contamination has been detected in Auger measurements during the time required for our experiments.

In this geometry and assuming that the buffer layer is stiff and infinitely thick relative to the AuNi film, the in-plane (biaxial) strain is imposed by the buffer layer and localized only in the AuNi layer. This in-plane *misfit* strain due to lattice mismatch may be written as

$$\varepsilon_{\mathrm{mis}} = \frac{a_s - a(x)}{a(x)}, \tag{1}$$

where a_s is the lattice parameter of the buffer layer, x is the Ni content and $a(x)$ is the lattice parameter of bulk metastable fcc AuNi solid solutions. The variation of $a(x)$ with the Ni content has been studied both experimentally[17] and theoretically.[19,28] The results show a positive deviation from Vegard's law.

The relevant parameter of this study is the effective inplane *residual* strain $\varepsilon_r^{\parallel}$ given by

$$\varepsilon_r^{\parallel} = \frac{a_{\parallel} - a(x)}{a(x)}, \tag{2}$$

where $a_{\parallel}$ is the in-plane lattice parameter of the AuNi epitaxial layer, measured using asymmetrical XRD. The value of $a_{\parallel}$ depends on the degree of the strain relaxation of the AuNi layer and is function, among others, of the AuNi layer thickness (h) and of a_s.

If the AuNi layer is *coherently strained*, i.e., no relaxation occurs, then $a_{\parallel} = a_s$ and the residual strain $\varepsilon_r^{\parallel}$ is equal to the misfit strain $\varepsilon_{\mathrm{mis}}$.

If the thickness of the AuNi layer is higher than a critical thickness depending on the Ni content and on the value of a_s, then partial relaxation may take place via the introduction

of defects (dislocation and/or twinning). In that case, the residual strain is lower than the misfit strain: $|\varepsilon_r^{\parallel}| < |\varepsilon_{\mathrm{mis}}|$. So the state of strain of the AuNi layer, given by the value of $\varepsilon_r^{\parallel}$, may be varied by changing (i) the value of a_s, i.e., the nature of the buffer (here Au, Pt, and Pd), for a fixed composition, (ii) the Ni content, i.e., the value of $a(x)$, for a given kind of buffer layer, (iii) the AuNi layer thickness (h)—to allow relaxation—for fixed values of a_s and $a(x)$.

The in-plane lattice parameters of the various buffer layers (a_s) and AuNi layers $(a_{\parallel})$ were deduced from XRD measurements around the $(\bar{1}\bar{1}3)$ Bragg reflection. The out-of-plane lattice parameters of the AuNi alloys $(a_{\perp})$ were measured from conventional θ–2θ XRD scans. The XRD measurements showed that the values of a_s for the 500 Å thick buffer layers were equal, within the limits of experimental precision (5.10^{-3} Å), to that of bulk values, respectively 4.078 Å, 3.889 Å, and 3.925 Å for Au, Pd, and Pt. The measured values of $a_{\parallel}$ and $a_{\perp}$ are reported in Table I for the AuNi alloys.

For the case of coherent layers, the Ni content may be estimated from the $a_{\parallel}$ and $a_{\perp}$ values of the AuNi layer, in the linear elasticity theory approximation. Assuming an homogeneous and tetragonal deformation of the AuNi layer and a zero stress of the σ_{zz} component, we have[47]

$$\varepsilon_r^{\perp} = -2 \frac{C_{12}(x)}{C_{11}(x)} \varepsilon_r^{\parallel}, \tag{3}$$

where

$$\varepsilon_r^{\perp} = \frac{a_{\perp} - a(x)}{a(x)} \tag{4}$$

is the out-of-plane residual strain and C_{11} and C_{12} are the elastic constants of the AuNi alloys. By using Eqs. (2)–(4), one obtains

$$a(x) = \frac{C_{11}(x)a_{\perp} + 2C_{12}(x)a_{\parallel}}{C_{11}(x) + 2C_{12}(x)}. \tag{5}$$

For simplicity we have used a linear variation of the elastic constants with the Ni content, while the variation of $a(x)$ takes into account the deviation from Vegard's law.[45] Once the experimental values of $a_{\parallel}$ and $a_{\perp}$ are determined, the Ni content x may be calculated from the implicit Eq. (5).

B. Samples description

Three sets of samples were elaborated at RT by codeposition of Au and Ni: (i) $Au_{1-x}Ni_x$ alloys with $0.14 < x < 0.5$ *coherently* grown on a Au (001) buffer, the corresponding thickness ranges between respectively 8 and 3.5 nm to avoid relaxation, (ii) $Au_{0.5}Ni_{0.5}$ and $Au_{0.6}Ni_{0.4}$ alloys *coherently* grown on Au, Pt, and Pd (001) buffers, and (iii) *partially relaxed* $Au_{0.5}Ni_{0.5}$ and $Au_{0.6}Ni_{0.4}$ alloys grown on a Au (001) buffer, with a thickness of about 35 nm.

In addition to alloys thin films, artificially modulated structures (AMS) were elaborated by MBE, with nominal periods different from those which have been observed in codeposited samples after annealing. AMS coherently grown on Au or Pd buffer layers and having an average Ni content of 0.4 and 0.5 were investigated to see if the period is

TABLE I. Samples characteristics: thickness (h), Ni content (x) deduced from the RHEED and XRD measurements, lattice parameters ($a_\parallel$ and $a_\perp$) measured from XRD, misfit strain (ε_{mis}) and effective residual strain ($\varepsilon_r^\parallel$)

Specimen	Buffer	h (nm) (± 0.2)	x RHEED	x XRD	$a_\parallel$ (Å) (± 0.005)	$a_\perp$ (Å) (± 0.005)	ε_{mis}	$\varepsilon_r^\parallel$ ($\pm 0.1\%$)	Coherency?
$Au_{0.87}Ni_{0.13}$	Au	8	0.14 ± 0.01	0.14 ± 0.01	4.074	3.934	1.4%	1.4%	Yes
$Au_{0.8}Ni_{0.2}$	Au	6	0.20 ± 0.01	0.19 ± 0.01	4.076	3.880	2.1%	2.1%	Yes
$Au_{0.7}Ni_{0.3}$	Au	6	0.28 ± 0.01	0.28 ± 0.01	4.072	3.787	3.2%	3.1%	Yes
$Au_{0.6}Ni_{0.4}$	Au	3.6	0.39 ± 0.01	0.40 ± 0.01	4.070	3.648	4.6%	4.4%	Yes
$Au_{0.5}Ni_{0.5}$	Au	3.5	0.49 ± 0.02	a	4.071	3.462	6.1%	5.9%	Yes
$Au_{0.6}Ni_{0.4}$	Pd	5		0.41 ± 0.01	3.884	3.891	-0.2%	-0.3%	Yes
$Au_{0.6}Ni_{0.4}$	Au	35		b	3.984	3.715	4.8%	2.4%	No
$Au_{0.5}Ni_{0.5}$	Pt	17		0.52 ± 0.01	3.937	3.683	2.8%	2.8%	Yes
$Au_{0.5}Ni_{0.5}$	Au	37		b	3.875	3.731	6.2%	0.9%	No
$(Au_1Ni_1)_{15}$	Au	5.2	0.5 ± 0.02	a	4.079	3.440	6.2%	6.2%	Yes
$[Ni_1/(Au_{0.7}Ni_{0.3})_6]_5$	Au	6.3	0.37 ± 0.02	a	4.064	3.593	4.4%	4.0%	Yes
$[Ni_1/(Au_{0.7}Ni_{0.3})_6]_5$	Pd	6.8	0.42 ± 0.02	a	3.896	3.891	-0.3%	-0.3%	Yes

[a]The linear elasticity limit is no longer valid.
[b]The strain is not homogeneous along the growth direction.

changed from the nominal one upon annealing. The growth of the AMS was achieved using the ''phase-locked'' epitaxy technique,[48] which proved to be a very efficient way of designing AuNi alloys in the $L1_0$ structure.[49]

The samples characteristics (thickness, composition, misfit strain, and residual strain) are reported in Table I. The composition values are those deduced from the RHEED measurements during growth (see Sec. IV A) and, for the case of coherent layers, from XRD measurements using Eq. (5).

C. Characterization

1. X-ray diffraction

Room temperature XRD measurements were performed with a conventional θ–2θ diffractometer equipped with a primary graphite monochromator selecting the Cu Kα radiation ($\lambda = 1.5418$ Å).

Another θ–2θ diffractometer operating with a secondary graphite monochromator was used for *in situ* temperature XRD experiments (see Fig. 4). The sample is fixed on a plane sample holder by a specially designed cover, which ensures thermal homogeneity around the sample. A thermocouple is placed in a channel grooved at the sample holder surface with its tip coming exactly behind the sample. A heating element and its regulating thermocouple are inserted in the sample holder shell. The whole set is fixed onto the vacuum chamber. Two windows covered with beryllium foils are cut in the chamber to allow the primary and secondary x-ray beams to go through. The vacuum level in the chamber reaches 10^{-9} Torr at RT and rises to some 10^{-8} Torr at 300 °C.

The sample positioning is accurately controlled at RT and at 100 °C. The displacement of the sample holder due to thermal dilatation has been calibrated versus the regulating temperature. Its variation is strictly linear in the 50–550 °C range with a slope of $1.003\ 10^{-6}$ m/ °C.

The sample holder temperature is permanently recorded. Its stability range is ± 0.5 °C during several hundreds hours. A gold layer deposited on a MgO substrate, then annealed, has been used to calibrate the equilibrium temperature on the sample surface versus the regulating temperature. Because of the measurement and calibration methods uncertainties, the sample temperature is known within ± 5 °C.

2. HREM

The samples were also characterized by HREM. For this purpose, plan view and cross-sectional specimens having [001] and [110] foil normals, respectively, were prepared by mechanical thinning followed by Ar ion milling. The HREM observations were carried out on a JEOL 4000EX microscope operating at 400 kV with a spherical aberration Cs = 1 mm and equipped with a top entry goniometer stage.
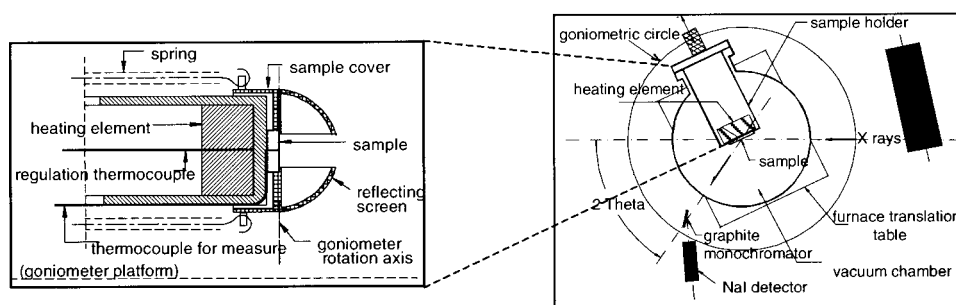
FIG. 4. *In situ* temperature XRD device: sample holder (left) and diffractometer (right).
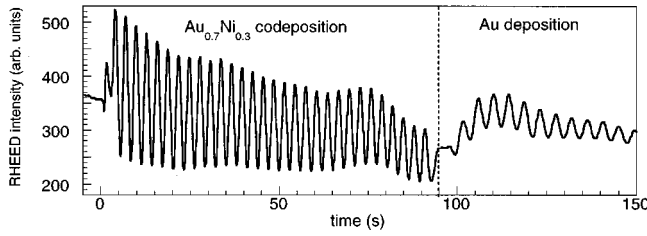
FIG. 5. Oscillations in RHEED intensity during the growth of the $Au_{0.7}Ni_{0.3}$ film on the Au (001) buffer layer and during the subsequent deposition of the Au capping layer. The vertical dashed line corresponds to the closure of the Ni shutter.

IV. RESULTS

A. As-grown samples

It has to be pointed out that the accurate control of the molecular fluxes during codeposition is usually a difficult procedure in MBE growth. In the case of the AuNi system, we have taken advantage of the high quality and reproducibility of the RHEED intensity oscillations to monitor the molecular fluxes towards an accurate control of the actual stoichiometry during the growth of the codeposited samples. The relative incertitude on the composition is estimated to be $\pm 4\%$ following this type of calibration.

Indeed, for all of the samples studied, the RHEED intensity of the specular reflection registered during the codeposition of Au and Ni shows strong and weakly damped oscillations (see Fig. 5), indicating a layer-by-layer growth mode. These oscillations are present up to 30–70 monolayers (ML) thickness, depending on the Ni content and surface quality of the buffer layer. Oscillations also occur during the sequential deposition of Au and Ni and are used for the feedback control of the opening and closure of the shutters (phase-locked epitaxy). This growth technique results in AMS with a good periodicity along the growth direction.

Oscillations in the RHEED intensity are also observed during the deposition of the Au capping layer, which shows that the growth is still two-dimensional and attests the good structural quality of the AuNi layer. In this case, the composition of the codeposited alloys may be deduced from the periods T_{AuNi} and T_{Au} measured during the respective growth of the AuNi and Au layers (see Fig. 5), according to the following equation:

$$x = 1 - \frac{T_{AuNi}}{T_{Au}}. \qquad (6)$$

The composition values calculated from Eq. (6) are reported in Table I. They are in close agreement with the ones deduced from XRD measurements and the difference with the nominal composition is less than 2 at. %.

The structural characterization of the as-grown specimens studied by XRD and HREM has been published elsewhere.[45,50,51] We will mention below the main results through the description of Fig. 6.

• Symmetrical XRD θ–2θ scans along the [001] direction of the Au buffer layer are shown on Fig. 6(a) for *coherent* and *partially relaxed* $Au_{0.6}Ni_{0.4}$ layers. The scans drawn on a decimal logarithmic scale exhibit, in addition to the (002) fundamental reflections of the MgO substrate and Au buffer
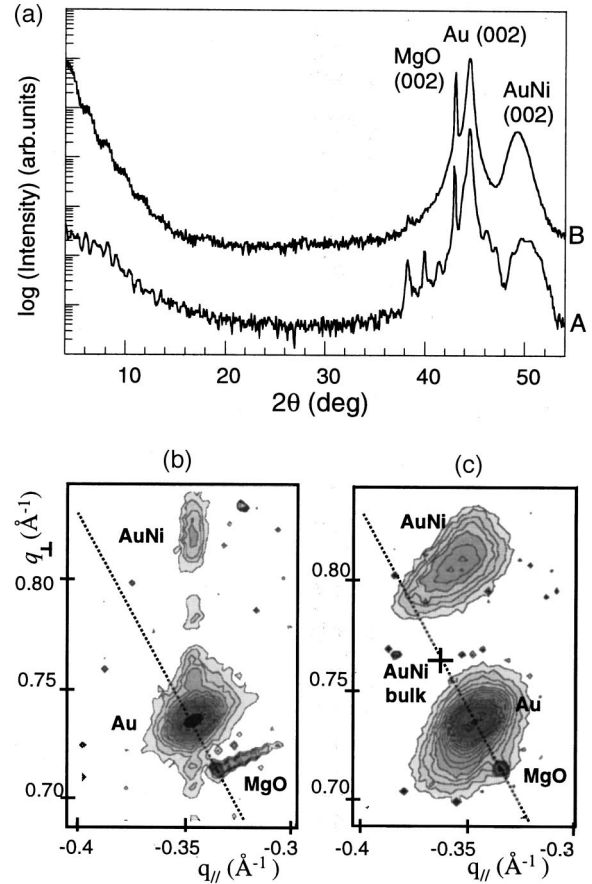
FIG. 6. (a) RT θ–2θ scans (decimal logarithmic scale) of the as-grown $Au_{0.6}Ni_{0.4}$ alloy grown on Au: coherent layer (curve A) and partially relaxed layer (curve B), (b) Iso-intensity reciprocal space map in the vicinity of the $(\bar{1}\bar{1}3)$ reflection for the coherent $Au_{0.6}Ni_{0.4}$ alloy, (c) Iso-intensity reciprocal space map in the vicinity of the $(\bar{1}\bar{1}3)$ reflection for the partially relaxed $Au_{0.6}Ni_{0.4}$ alloy.

layer, only one single (002) AuNi peak, indicating that the MBE codeposition of Au and Ni does stabilize a solid solution. For the coherent layer, the AuNi (002) peak is large because of the thin thickness of the layer (3.6 nm) and is also modulated in intensity due to the interferences with the diffracted intensity of the capping layer. For the case of the partially relaxed layer, because the thickness is higher (36 nm), the (002) peak has a well-defined form. At low angles, interferences between the reflected beam at the top surface and the reflected beam(s) at the bottom interface(s), known as Kiessig's fringes, are observable in both cases. In some samples, a weak Au (111) peak is observed near $2\theta = 38°$ and probably comes from incoherent growth regions on the MgO substrate.

• The XRD maps around the $(\bar{1}\bar{1}3)$ reflections are presented on Fig. 6(b) and 6(c). For the 3.6 nm-thick layer, the in-plane coherency is attested by the same value of the in-plane scattering vector $q_\parallel$ of the Au and AuNi peaks. Moreover, the AuNi layer is under a tetragonal distortion ($a_\perp < a_\parallel$) since the AuNi peak is not located on the dashed line representing the locus of points for which $a_\parallel = a_\perp$, i.e., relaxed layers with cubic symmetry. HREM images[50] confirm that the AuNi layer is homogeneous and coherently strained and no defects have been detected. For the 36 nm-thick layer, the
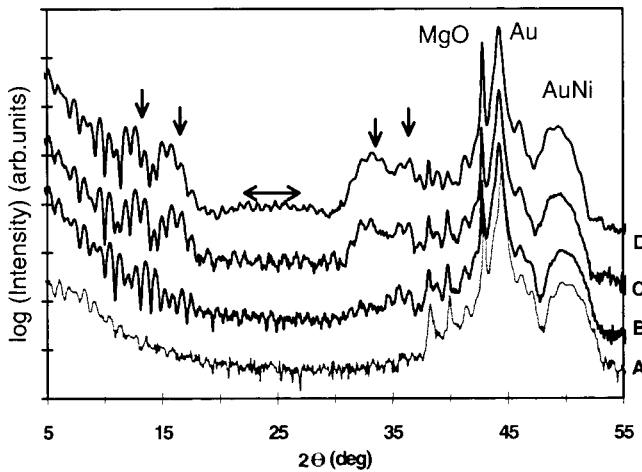
FIG. 7. Evolution of the θ–2θ scans during the annealing of the Au$_{0.6}$Ni$_{0.4}$ film coherently grown on Au (001): (A) at RT, (B) after 4.7 h at 202 °C, (C) after 90 h at 202 °C, (D) after 540 h at 202 °C.

relaxation occurs via the introduction of $a/6\langle 112 \rangle$ partial dislocations on {111} gliding planes. These dislocations generate stacking faults as well as microtwins, which are made up of an agglomeration of $a/6\langle 112 \rangle$ partials.[45] But the AuNi layer has not entirely relaxed since the $(\bar{1}\bar{1}3)$ AuNi peak differs from the $(\bar{1}\bar{1}3)$ AuNi bulk position located on the dashed line. The AuNi layer is therefore partially relaxed and a relatively high residual strain is still present ($\varepsilon_r^{\parallel} = 3.0\%$). The state of coherency of the different samples is reported in Table I.

B. Annealing effects

The structural evolution upon annealing of codeposited Au$_{1-x}$Ni$_x$ solid solutions coherently grown on Au(001) has been first described in Refs. 25 and 51. We will just recall the results obtained on the coherent Au$_{0.6}$Ni$_{0.4}$ alloy ($h = 3.6$ nm, $\varepsilon_r^{\parallel} = 4.4\%$) with the help of Fig. 7, which describes the general evolution of the θ–2θ scans with temperature. A significant evolution was observed for annealing above 200 °C. Below this temperature, the time required for an observable modification is too long (more than 300 h). Two regimes may be pointed out:

(1) In the 200–240 °C range, a modification of the x-ray diffraction spectrum is noted in the first hours and continues to develop. After about ten hours (curve B), two main features are observed: more pronounced Kiessig's fringes at low angles, indicating an improvement in the structural quality of the sample, and one or two sets of superlattice peaks ($\downarrow$) arising from a compositional modulation along the growth direction. The intensity of these additional peaks is also modulated by interference effects due to the finite thickness of the AuNi layer, as explained in Sec. IV A.

For the case of the Au$_{0.6}$Ni$_{0.4}$ alloy grown on Au, two sets of superstructure peaks are observable (curves C and D). They may be related to the coexistence of two different superlattice periods, respectively 3 and 3.8 ML. About the latter noninteger period, we have shown[51] that a noninteger period in the XRD spectrum may be well reproduced by a simulation on a structural model consisting of a mixture of

two kinds of modulated domains having two different integer periods, respectively 3 and 4 ML for the present case. The atomic structure of these modulated domains has also been refined and the result gives a mixture of two atomic periodic stackings made up with atomic superstructures having respectively 1 Ni-rich plane/2 Au-rich planes and 1 Ni-rich plane/3 Au-rich planes. The compositional total amplitude is in both cases higher than 80 at. % in order to reproduce the superstructure peak intensities. The noninteger period noticed in the XRD spectrum comes from the statistical mixture of these two different periodic structures. Indeed the XRD pattern will reproduce either the sum of the diffracted intensities—distinct peaks are therefore observed—or the sum of the diffracted amplitudes—an average broad peak is therefore observed—depending on the size of the domains compared with the lateral coherency length of the x-ray beam (which we have calculated to be about 20 nm). The broad contribution at midangles ($\leftrightarrow$) is reproduced by the simulation and is related to this statistical distribution of periods. This lateral structure with domains of different sizes and periods is confirmed by HREM observations.[50]

The intensity of the superlattice peaks increases with time until it reaches an asymptotic value. Beyond 300 h, the intensity ratio I_s/I_f, where I_s and I_f are, respectively, the intensity of the satellite and fundamental reflections, no longer evolves. This indicates that a stable state has been reached. For the case of the Au$_{0.6}$Ni$_{0.4}$ film, it may be noted that after about 90 h the intensity of the 3 ML period set becomes greater than that of the 3.8 ML period set, which may indicate that the 3 ML period domains have grown to the detriment of the 4 ML period ones.

No evolution of the period with the time and temperature is found with any sample.

(2) At 240 °C the AuNi (002) peak shifts towards the Au (002) peak but the superlattice peaks are still present. For longer times, the intensity of the superlattice peaks begins to decrease and the AuNi (002) peaks is no more separable from the Au (002) peak. These effects may be explained by the Ni bulk diffusion from the alloy layer towards the buffer and capping layer, which contributes progressively to the disappearance of the modulated structure. The final state is a Ni dilute solid solution. No demixtion is observed with any sample.

C. Strain effect

The role of the epitaxial strain was studied on a Au$_{0.6}$Ni$_{0.4}$ alloy for three specimens having different residual strain: specimen A ($h = 5$ nm, $\varepsilon_r^{\parallel} = -0.3\%$) coherently grown on Pd, specimen B ($h = 35$ nm, $\varepsilon_r^{\parallel} = 3.0\%$) partially relaxed on Au and specimen C ($h = 3.6$ nm, $\varepsilon_r^{\parallel} = 4.4\%$) coherently grown on Au. The θ–2θ scan recorded on the specimen A is shown on Fig. 8 after 90 h at 220 °C (curve A). It seems clear from curve A that some minimum strain is required for the modulated structure to develop: with the Pd buffer, no superlattice peak is observed after an annealing time of 300 h, but only interfaces sharpening, while satellite peaks were observed for the same alloy grown on Au (curve C). Annealing at a higher temperature leads to the bulk diffusion of Ni.

For the partially relaxed alloy, the θ–2θ scan recorded after 90 h at 220 °C (curve B) displays well-defined satellite peaks. They result from a compositional modulation having a
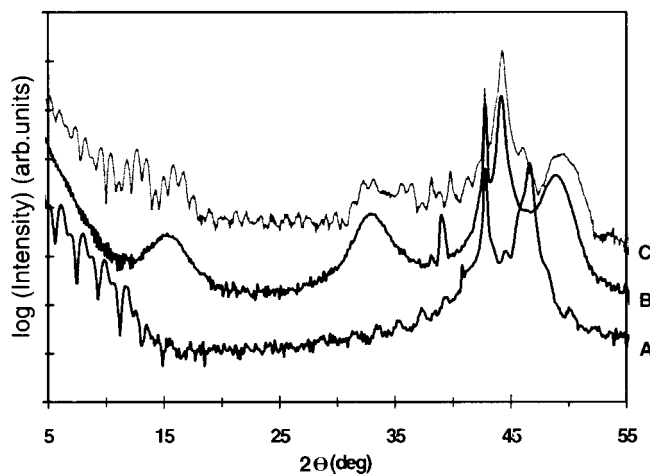
FIG. 8. Influence of the residual strain for a fixed alloy composition $x=0.4$: evolution of the $\theta-2\theta$ scans after 90 h at 220 °C recorded for (A) the coherent layer grown on Pd (001) and for (B) the partially relaxed layer grown on Au (001). The curve C corresponds to the coherent $Au_{0.6}Ni_{0.4}$ film [same curve as Fig. 7(C)] is shown for comparison.

periodicity of 3.1 ML, close to the one observed for the coherent layer (curve C). Simulation of the XRD spectrum confirms that the composition profile is asymmetrical:1 Ni-rich plane ($x=0.72$) and 2.1 Au-rich planes ($x=0.24$). Nevertheless, the width of the satellite peaks is greater and the intensity ratio I_s/I_f is lower. Therefore, it may be inferred that the size of the ordered domains is lower than the one observed for the coherent layer. This statement is confirmed by HREM observation: Fig. 9 shows a cross-sectional view of the partially relaxed AuNi layer along the $\langle 110 \rangle$ direction.
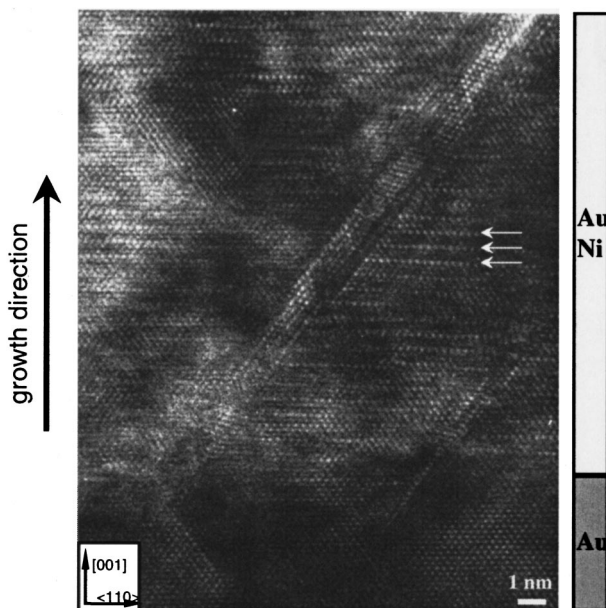
FIG. 9. [110] cross-section HREM image of the partially relaxed $Au_{0.6}Ni_{0.4}$ layer grown on Au (001), after a heat treatment at 220 °C for 360 h (courtesy of J. Thibault). Part of the misfit strain has been relaxed by twins on {111} planes. Inside the AuNi layer, a periodic modulation of the contrast is observed along the growth direction (see the arrows).
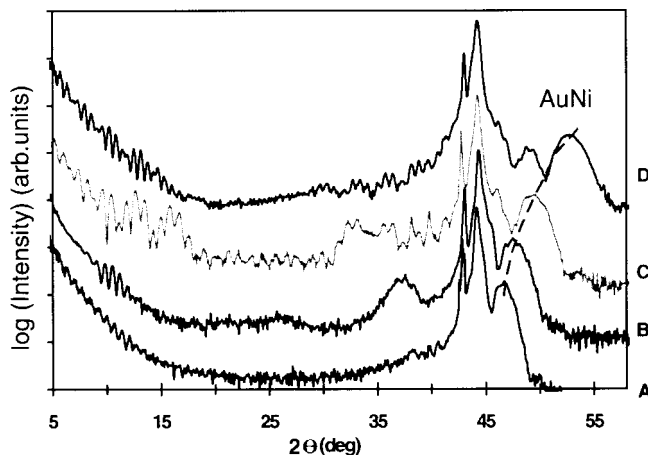
FIG. 10. Influence of the composition for a given in-plane lattice parameter $a_\parallel=4.07$ Å: evolution with temperature of the $\theta-2\theta$ scans recorded for (A) the $Au_{0.8}Ni_{0.2}$ film after 65.4 h at 220 °C, (B) the $Au_{0.7}Ni_{0.3}$ film after 94 h at 220 °C, (C) the $Au_{0.6}Ni_{0.4}$ film after 90 h at 202 °C and (D) the $Au_{0.5}Ni_{0.5}$ film after 150 h at 208 °C.

A modulated structure with a periodicity of 3 ML is clearly visible along the growth direction, but within small domains (5 to 8 nm in lateral size): the contrast of the HREM image is made up of one bright and two darker atomic planes, corresponding, respectively, to 1 Ni-rich plane and 2 Au-rich planes. The lateral extension of the domains is limited by twins along {111} planes, which have contributed to relax part of the misfit strain imposed by the Au buffer layer. It would be interesting to know what would occur for a fully relaxed AuNi layer. But this would require the growth of a very thick layer, which is not without practical difficulty in MBE.

D. Composition effect

The influence of the composition was studied on several $Au_{1-x}Ni_x$ alloys coherently grown on Au. The composition range used in the present study is 0.14–0.5, the corresponding residual strain range being 1.4–5.9 %. For higher compositions, the required thickness to keep coherency is too low to detect significant evolutions of the XRD scans. For $x=0.14$ and $x=0.19$, no composition modulation was observed after 150 h at several temperature stages, ranging from 220 °C to 250 °C (see curve A of Fig. 10). For $0.28<x<0.5$, satellite peaks were observed and the period of the modulated structure is found to decrease with the Ni content: 4.4 ML for $x=0.28$ to about 3 ML for $x=0.5$.

The curve B of Fig. 10 shows the $\theta-2\theta$ scan of the $Au_{0.7}Ni_{0.3}$ alloy ($h=6.0$ nm, $\varepsilon_r^\parallel=3.1\%$) after annealing at 220 °C. The average period is 4.4 ML and corresponds to ordered domains having either a 1 Ni-rich plane/3 Au-rich planes structure or a 1 Ni-rich plane/4 Au-rich planes structure. The curve C of Fig. 10 corresponds to the $\theta-2\theta$ scan of the $Au_{0.6}Ni_{0.4}$ alloy and has been described above (same curve as Fig. 7(C)). For the $Au_{0.5}Ni_{0.5}$ alloy ($h=3.5$ nm, $\varepsilon_r^\parallel=5.9\%$) after annealing at 208 °C during 150 h, several additional peaks are visible between $2\theta=8°$ and 16° and between $2\theta=28°$ and 38° (curve D). They are related to interference fringes, as confirmed by a Fourier analysis of the $\theta-2\theta$ scan: the two main contributions in the diffracted intensity arise from layers having a characteristic thickness of 3.5 ± 0.1 nm and 12.2 ± 0.1 nm, which corresponds, respec-
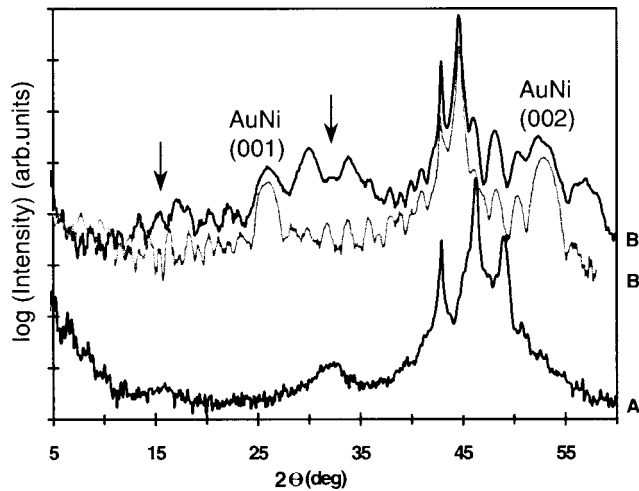
FIG. 11. θ–2θ scan recorded for the $Au_{0.5}Ni_{0.5}$ film grown on Pt, after 187 h at 216 °C (A) as compared to the θ–2θ scan recorded for the $(Au_1Ni_1)_{15}$ AMS grown on Au, after 0.7 h (B) and 376 h (B′) at 216 °C.

FIG. 12. Variation of the period of the modulated structure with the Ni content: coherent layers ($\blacklozenge$), partially relaxed layers ($\diamond$), and AMS ($\times$, initial state), ($\bigcirc$, final state).

tively, to the thickness of the alloy and the capping layer. However, these fringes are not visible on the scan *before* annealing because they are too weak. Thus, without the presence of an additional contribution near 12° and 32°, which would increase the background level intensity, these fringes would not be visible. By analogy with the previous results, this contribution may be attributed to the development of a modulated structure. The period is estimated to be 3.0 ± 0.5 ML due to the uncertainty in the determination of the position of the superstructure peaks.

The same $Au_{0.5}Ni_{0.5}$ alloy was coherently grown on a Pt(001) buffer, but with a thickness of 17 nm due to the smaller imposed misfit strain ($\varepsilon_{mis} = 2.8\%$). We have seen previously that varying the imposed strain without changing the Ni content doesn't affect the superstructure period but the size and the volume of the ordered domains. The scan recorded after annealing at 216 °C reported on Fig. 11 (curve A) shows two satellite peaks, the position of which corresponds to a 3.0 ML period modulated structure, in close agreement with the one deduced from Fig. 10 (curve D). Rocking-curves measurements reveal that the width of the satellite peaks is high ($\Delta\theta = 4.8°$) compared to the AuNi (002) one (0.43°). This means that the coherency length of the ordered domains is low (about 3 nm).

E. Stability of the modulated structure

In order to determine whether these modulated structures are a new-ordered phase or an intermediate state towards further decomposition, we have studied the structural evolution of AMS having a periodicity very different from the one coming out upon the annealing of the codeposited alloys. We report on Fig. 11 the results obtained from the $(Au_1Ni_1)_{15}$ AMS, corresponding to a 2 ML period structure ($L1_0$-type). The scan recorded on the as-grown sample reveals the presence of a strong (001) AuNi reflection. The long-range order parameter, extracted from the integration of the superlattice peaks (001) and (003) and two fundamental reflections (002) and (004), is 0.38. During annealing, the intensity of the (001) superlattice peak decreases and a new
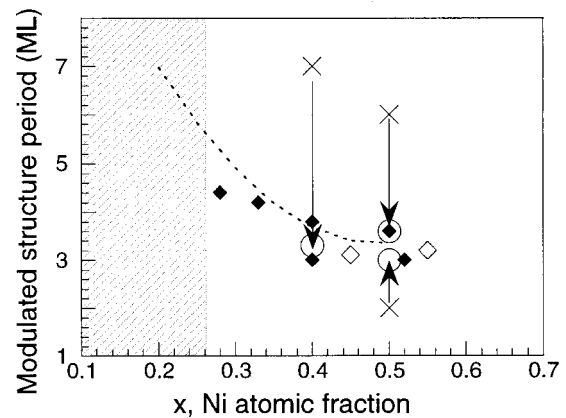
contribution related to the development of a 3.0 ML period structure appears (see curves B and B′).

In conclusion, the artificial period imposed to the AuNi layer doesn't alter the period of the modulated structure observed upon annealing. This means that the modulated structure is a stable state of the strained AuNi alloy, in a relatively limited range of temperature. To confirm this assumption, two other AMS were elaborated with a Ni average composition equal to 0.4, on Au and Pd buffer layers. The stacking is $[Ni_1/(Au_{0.7}Ni_{0.3})_6]_5$ and the thickness is 6.5 nm. The residual strain is 3.9% for the layer coherently grown on the Au buffer and -0.3% for the one grown on the Pd buffer. The AMS grown on Au evolves towards a 3.3 ML period modulated structure whereas the same AMS grown on Pd evolves towards a stable solid solution.[52] These observations confirm (i) the stability of the modulated structure and (ii) that it is strain driven.

F. Summary

The *in situ* temperature diffraction experiments performed on several samples sets with different residual strains and initial configurations (coherent and partially relaxed alloys, artificially modulated structures) have shown that a strain-driven modulated structure, consisting of the alternation of 1 Ni-rich plane / 2 or 3 Au-rich planes, develops upon annealing between 200 and 240 °C. The whole results are synthesized on Figs. 12 and 13, which display the variation of the period versus the Ni content and versus the residual strain. It may be seen that (1) the period is essentially Ni-content dependent even if the period variation range is narrow and (2) a threshold strain is necessary for the modulated structure to appear.

V. DISCUSSION

A. Comparison with the bulk state

In the bulk state, such modulated structures have been observed along the three $\langle 100 \rangle$ directions, either by XRD (Refs. 21, 26, 53) or by transmission electron microscopy,[20,22,54] on AuNi metastable alloys obtained by rapid quenching and annealed below 300 °C. The evolution of the
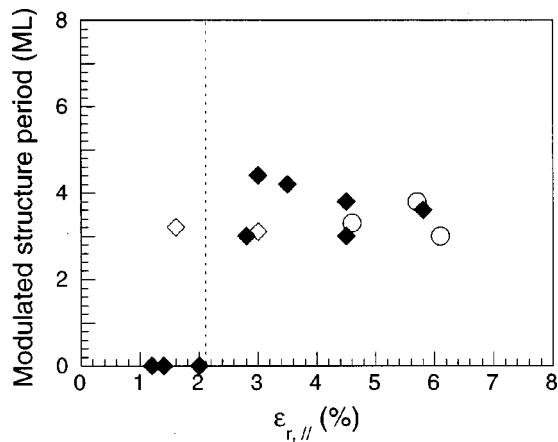
FIG. 13. Variation of the period of the modulated structure with the residual strain: coherent layers ($\blacklozenge$), partially relaxed layers ($\lozenge$), and AMS ($\bigcirc$, final state).

wavelength with the Ni content is reproduced on Fig. 12 (dashed line). In the range of high-Ni content ($x > 0.3$), the variation is consistent with our observations on thin alloy films. But for $x < 0.3$, we do not detect the development of modulated structures inside the AuNi layers, whereas long-period compositional modulations have been reported in the bulk state. In addition, the compositional amplitude deduced from the simulations of the $\theta-2\theta$ scans is large (~ 50 to 80 at. %), while, in bulk alloys, Woodilla and Averbach[20] estimated it to about 5 at. %. This explains why our XRD scans display well-defined superstructure peaks whereas broad and weak satellite peaks were observed in bulk specimens.[53]

But the involved mechanisms have not up to now been clearly identified. Some authors[20,22] put forward a spinodal decomposition mechanism, others[26] a clustering process, which gives rise to Ni monoatomic platelets.

In the present study, two remarks may be stated: (1) the period of the modulated structure does not evolve with time neither with temperature, as it would be expected if a spinodal decomposition mechanism occurred[23] (2) a threshold residual epitaxial strain is necessary for the modulated structure to develop, but beyond this threshold, the period varies essentially between 3 and 4 ML (see Fig. 13). We have recently studied the influence of the epitaxial strain on the spinodal decomposition.[19] Our model is an extension of Cahn's original theory. We have included in the expression of the total free energy the contribution due to the coherent epitaxy on to a substrate. We obtain a significant evolution of the composition fluctuation period with the substrate lattice parameter. For example, for $x = 0.4$, the period is found to increase from 6.0 ML for $a_s = 4.08$ Å (Au substrate), to 20 ML for $a_s = 3.92$ Å (Pt substrate) and over 30 ML for $a_s = 3.89$ Å (Pd substrate). Such a variation is not observed experimentally. We may therefore infer from the results (1) and (2) that a spinodal decomposition mechanism does not satisfactorily explain the origin of the modulated structures observed in our samples.

Besides, Dressler *et al.* have performed *in situ* HREM experiments to observe the first stages of the phenomenon.[55] Preliminary results show that Ni-rich platelets, 5 nm in size, nucleate inside the AuNi layer. Then, their lateral size increases up to 20 nm during annealing. These Ni-rich platelets

seem to be the precursors of the modulated structures that we observe from XRD, once a periodicity along the growth direction has been established. These monoatomic platelets could be related to the formation of Guinier-Preston zones, as it is the case in the bulk Al-Cu system.[56,57] In this system, precipitation of monoatomic Cu platelets occurs for heating treatment below 150 °C. The structure subsequently evolves towards the formation of θ' (Al_2Cu) and θ'' ($Al_3Cu, Z_{1,3}$ structure) ordered phases. But the elementary mechanisms governing the transformation stages are not well identified and can therefore be hardly transposed to thin films case.

B. Epitaxial strain ordering

The results obtained on the AMS clearly demonstrate that a stable phase with a periodicity between 3 and 4 ML is obtained under high enough epitaxial strain. This acts in favor of a strain-stabilized ordering process, based on nucleation and growth mechanisms. We have seen in Sec. II that tetragonal-ordered structures are expected to be stabilized under large biaxial expansion. Experimentally, we obtain a threshold residual strain of $\varepsilon_r^{\parallel} = 2\%$, which corresponds, for $x = 0.4$, to a substrate lattice parameter $a_s = 3.97$ Å, close to the theoretical value calculated for a $L1_0$ structure (3.95 Å). In the bulk state, a threshold strain cannot be defined explicitly but some internal stresses, originating from the quenching process, are obviously present and could therefore favor the development of compositional modulations along the three $\langle 001 \rangle$ elastic soft directions.

The modulated structure, which consists of a periodic alternation of 1 Ni-rich plane/2 or 3 Au-rich planes may probably be identified to a $Z_{1,3}$ or $Z_{1,4}$-ordered structure, depending on the Ni content. To check this hypothesis, we have performed numerical simulations to study the stability of $Z_{1,n}$-type ordered structures coherently strained on a Au buffer layer. We have considered three different average Ni contents: $x = 0.3$, 0.4, and 0.5. As it is observed experimentally, the modulated structure is not made up of pure Au or Ni planes. Therefore the possibility of mixing the atoms on the different planes of the $Z_{1,n}$-type structure has to be included in the calculation. This can be realized easily by numerical simulation using the TB interatomic potentials described in Sec. II. The Ni content on each plane of the $Z_{1,n}$ structure is calculated from the average composition x and the period ($n+1$) of the $Z_{1,n}$ structure. The results are reported on Fig. 14. For $x = 0.5$, the $L1_0$ structure has the lowest energy among the different ordered structures considered. For $x = 0.4$ or $x = 0.3$, the $Z_{1,2}$ or $Z_{1,3}$-ordered phase becomes energetically more favorable than the $L1_0$ structure. These calculations clearly suggest that during annealing one of these $Z_{1,n}$ structures may be selected depending on the Ni content. The general trend may be the following one: 1 atomic Ni plane is periodically phase-separated to decrease the total elastic contribution of the total free energy. Therefore the selected period may be the one that minimizes the Ni content on the remaining n Au-rich planes. This satisfactorily explains the experimental results but the agreement is not fully quantitative, since the experimental values of the periods are systematically shifted by $+1$ ML in comparison with
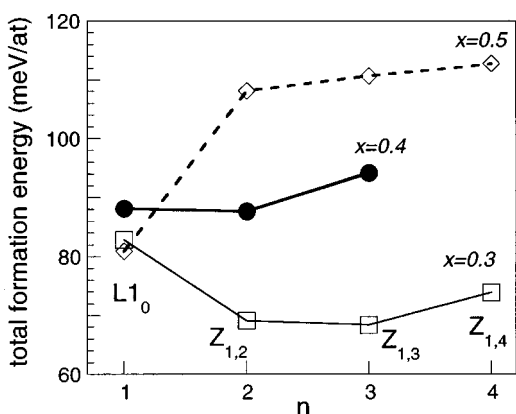
FIG. 14. Total formation energy calculated at $T = 0$ K for several $Z_{1,n}$-type ordered structures coherently strained on a Au buffer layer and having three different average Ni contents: 0.3, 0.4, and 0.5.

the expected periods deduced from our calculations. We have not for the moment a clear explanation for this slight deviation.

VI. SUMMARY AND CONCLUSIONS

Despite a strong phase-separation tendency in the bulk state, metastable (001) AuNi alloyed thin films may be elaborated by MBE. We have investigated the influence of the epitaxial strain on the structural evolution with temperature. Numerous specimens with different structures (solid solutions and AMS) and various Ni contents (0.14 to 0.5) were deposited on several buffer layers (Au, Pd, and Pt) in order to vary the residual epitaxial strain. The two relevant parameters of the study are the composition and the residual strain, which have been both carefully controlled by RHEED during the growth process. The samples were characterized by temperature XRD and HREM. It has been evidenced that, upon annealing between 200 and 240 °C, these out-of-equilibrium

AuNi alloys evolve towards a modulated structure along the growth direction, provided that the residual strain is high enough. The period of the modulated structure is between 3 and 5 ML, depending on the Ni content. It doesn't evolve with time neither with temperature. The compositional amplitude of these chemical modulations is large (more than 50 at. %) and the chemical profile is asymmetrical: 1 Ni-rich plane and 2 or 3 Au-rich planes.

The origin of this phenomenon has been discussed and compared with the observations on AuNi bulk samples reported in the literature. We suggest that a strain-stabilized ordering process occurs rather than a spinodal decomposition mechanism. Numerical simulations based on interatomic potentials within the tight binding scheme were performed in order to calculate the total formation energy (under epitaxial strain) of $Z_{1,n}$-type ordered compounds. The calculations satisfactorily explain the experimental results, though the agreement is not fully quantitative regarding the exact period of the modulated structure. We probably face with the limits of the computational techniques: (i) in first-principles methods, energy calculations under epitaxial strain are extremely time-consuming besides the fact that compositional fluctuations cannot be taken into account, and (ii) in semiempirical interatomic potentials, the finite range of the interactions up to the third or the fourth nearest-neighbors limits their ability to reproduce accurately the energy of long-period ordered compounds. Therefore, the results obtained in the AuNi system could be a promising challenge to improve the current state-of-the-art in computational methods.

*Present address: Laboratoire de Métallurgie Physique, Université de Poitiers, SP2MI, Téléport 2, bvd Marie et Pierre Curie, 86962 Futuroscope cedex, France.
Electronic address: gregory.abadias@lmp.univ-poitiers.fr

[1] G. A. Prinz, Phys. Rev. Lett. **54**, 1051 (1985).

[2] Z. Q. Wang, S. H. Lu, Y. S. Li, F. Jona, and P. M. Marcus, Phys. Rev. B **35**, 9322 (1987).

[3] A. Ourmazd and J. C. Bean, Phys. Rev. Lett. **55**, 765 (1985).

[4] T. S. Kuan, T. F. Kuech, W. I. Wang, and E. L. Wilkie, Phys. Rev. Lett. **54**, 201 (1985).

[5] D. Korakakis, K. F. Ludwig, and T. D. Moustakas, Appl. Phys. Lett. **71**, 72 (1997).

[6] V. Pierron-Bohnes, N. Ringelstein, A. Michel, S. Boukari, L. Bouzidi, N. Persat, E. Beaurepaire, M. Hehn, D. Muller, and M. C. Cadeville, J. Magn. Magn. Mater. **165**, 176 (1997).

[7] A. Marty, B. Gilles, G. Patrat, J. C. Joud, and A. Chamberod, in *Evolution of Surface and Thin Film Microstructure*, edited by H. A. Atwater *et al.*, MRS Symposia Proceedings No. 280 (Materials Research Society, Pittsburgh, 1993), p. 457.

[8] M. J. Jou, Y. T. Cherng, H. R. Jen, and G. B. Stringfellow, Appl. Phys. Lett. **52**, 549 (1987).

[9] G. L. Zhou, M. H. Yang, and C. P. Flynn, Phys. Rev. Lett. **77**, 4580 (1996).

[10] C. P. Flynn, Phys. Rev. Lett. **57**, 599 (1986).

[11] D. M. Wood and A. Zunger, Phys. Rev. B **40**, 4062 (1989).

[12] H. Reichert, S. C. Moss, P. Imperatori, and K. Evans-Lutterodt, Appl. Phys. Lett. **74**, 531 (1999).

[13] M. A. Herman and H. Sitter, in *Molecular Beam Epitaxy: Fundamentals and Current Status*, edited by M. B. Panish, Springer Series in Materials Science Vol. XII (Springer-Verlag, Berlin, 1996).

[14] J. L. Stevens and R. Q. Hwang, Phys. Rev. Lett. **74**, 2078 (1995).

[15] L. Bouzidi, V. Pierron-Bohnes, O. Haemmerlé, C. Bouillet-Ulhaq, and M. C. Cadeville, Thin Solid Films **318**, 215 (1998).

[16] H. Okamoto and T. B. Massalski, *Binary Alloy Phase Diagrams* (American Society for Metals, Metals Park, OH, 1986).

[17] E. C. Elwood and K. Q. Bagley, J. Inst. Met. **80**, 617 (1952).

[18] B. Golding and S. C. Moss, Acta Metall. **15**, 1239 (1967).

[19] G. Abadias, A. Marty, and B. Gilles, Acta Mater. **46**, 6403 (1998).

[20] J. E. Woodilla and B. L. Averbach, Acta Metall. **16**, 255 (1968).

[21] S. C. Moss, in *Local Atomic Arrangements Studied by X-ray Diffraction*, edited by J. B. Cohen and J. E. Hilliard (Gordon and

Breach, New York, 1966), p. 95.

[22] H. Hofer and P. Warbichler, Z. Metallkd. **76**, 11 (1985).

[23] J. W. Cahn, Trans. Soc. Min. Eng. AIME **242**, 166 (1968); Acta Metall. **14**, 1685 (1966).

[24] G. Renaud, M. Belakhovsky, S. Lefebvre, and M. Bessiere, J. Phys. III **5**, 1391 (1995).

[25] C. Dressler, G. Abadias, P. Bayle-Guillemaud, A. Marty, I. Schuster, J. Thibault, and B. Gilles, Appl. Phys. Lett. **72**, 2241 (1998).

[26] T. B. Wu and J. B. Cohen, Acta Metall. **31**, 1929 (1983).

[27] T. B. Wu and J. B. Cohen, Acta Metall. **32**, 861 (1984).

[28] J. Eymery, F. Lançon, and L. Billard, J. Phys. I **3**, 787 (1993).

[29] C. Colinet, J. Eymery, A. Pasturel, A. T. Paxton, and M. van Schilfgaarde, J. Phys.: Condens. Matter **6**, L47 (1994).

[30] C. Amador and G. Bozzolo, Phys. Rev. B **49**, 956 (1994).

[31] T. Deutsch and A. Pasturel, in *Stability of Materials*, Vol. 355 of *NATO Advanced Study Institute, Series B: Physics*, edited by A. Gonis *et al.* (Plenum, New York, 1996), p. 381.

[32] C. Wolverton and A. Zunger, Comput. Mater. Sci. **8**, 107 (1997).

[33] V. Ozolins, C. Wolverton, and A. Zunger, Phys. Rev. B **57**, 6427 (1998).

[34] C. Wolverton, V. Ozolins, and A. Zunger, Phys. Rev. B **57**, 4332 (1998).

[35] R. R. Hultgren, P. D. Andersen, and K. K. Kelley, *Selected Values of Thermodynamic Properties of Metals and Alloys* (Wiley, New York, 1963).

[36] P. A. Flinn, B. L. Averbach, and M. Cohen, Acta Metall. **1**, 664 (1953).

[37] T. Deutsch, P. Bayle, F. Lançon, and J. Thibault, J. Phys.: Condens. Matter **7**, 6407 (1995).

[38] G. Abadias, T. Deutsch, A. Marty, and B. Gilles (unpublished).

[39] V. Ozolins, C. Wolverton, and A. Zunger, Phys. Rev. B **57**, 4816 (1998).

[40] P. Alippi, P. M. Marcus, and M. Scheffler, Phys. Rev. Lett. **78**, 3892 (1997).

[41] P. M. Marcus and P. Alippi, Phys. Rev. B **57**, 1971 (1998).

[42] B. Gilles, A. Marty, G. Patrat, J. L. Vassent, J. C. Joud, and A. Chamberod, in *Mechanisms of Thin Film Evolution*, edited by S. M. Yalisove, C. V. Thompson, and D. J. Eaglesham, MRS Symposia Proceedings No. 317 (Materials Research Society, Pittsburgh, 1994), p. 621.

[43] P. Bayle, T. Deutsch, B. Gilles, F. Lançon, A. Marty, and J. Thibault, Ultramicroscopy **56**, 94 (1994).

[44] The buffer layer was thick enough to be completely relaxed, as it was verified by x-ray diffraction measurements.

[45] M. Dynna, A. Marty, B. Gilles, and G. Patrat, Acta Mater. **44**, 4417 (1996).

[46] D. Gibbs, B. M. Ocko, D. M. Zehner, and S. G. J. Mochrie, Phys. Rev. B **42**, 7330 (1990).

[47] D. J. Bottomley, P. Fons, and D. J. Tweet, J. Cryst. Growth **154**, 401 (1995).

[48] T. Sakamoto, H. Funabashi, K. Ohta, T. Nakagawa, N. J. Kawai, T. Kojima, and Y. Bando, Superlattices Microstruct. **1**, 347 (1985).

[49] M. Dynna, A. Marty, B. Gilles, and G. Patrat, Acta Mater. **45**, 257 (1997).

[50] P. Bayle-Guillemaud, C. Dressler, G. Abadias, and J. Thibault, Thin Solid Films **318**, 209 (1998).

[51] G. Abadias, I. Schuster, B. Gilles, and A. Marty, Thin Solid Films **318**, 204 (1998).

[52] G. Abadias, I. Schuster, B. Gilles, A. Marty, and T. Deutsch (unpublished).

[53] S. C. Moss and B. L. Averbach, in *Proceedings of the Conference on Small Angle Scattering of X-rays*, edited by H. Brumberger *et al.* (Gordon and Breach, New York, 1967), p. 335.

[54] Y. Fukano, J. Phys. Soc. Jpn. **16**, 1195 (1961).

[55] C. Dressler, P. Bayle-Guillemaud, and J. Thibault, Mater. Sci. Forum **294-296**, 321 (1999).

[56] H. Fujita, H. Nakayama, and Y. Fuchida, Philos. Mag. A **59**, 873 (1989).

[57] H. Fujita and C. Lu, Mater. Trans., JIM **33**, 897 (1992).